

Nonlinear Dynamics Chaotic and 177 Complex Systems

Proceedings of an International Conference
held in Zakopane, Poland
November 7–12, 1995
Plenary Invited Lectures

Edited by

E. INFELD

Sołtan Institute for Nuclear Studies, Warsaw, Poland

R. ŻELANZNY

Institute of Plasma Physics and Laser Microfusion, Warsaw, Poland

A. GAŁKOWSKI

Institute of Plasma Physics and Laser Microfusion, Warsaw, Poland



CAMBRIDGE
UNIVERSITY PRESS

The p
dyna
const
deve
It tur
unde
degr
unive
impl
impo
chem
othe

In th
math
in th
bas
into
theo
dyna
foun
and
an in

This
stud
inter
com

PUBLISHED BY THE PRESS SYNDICATE OF THE UNIVERSITY OF CAMBRIDGE
The Pitt Building, Trumpington Street, Cambridge CB2 1RP United Kingdom

CAMBRIDGE UNIVERSITY PRESS
The Edinburgh Building, Cambridge CB2 2RU, United Kingdom
40 West 20th Street, New York, NY 10011-4211, USA
10 Stamford Road, Oakleigh, Melbourne 3166, Australia

© Cambridge University Press 1997

This book is in copyright. Subject to statutory exception
and to the provisions of relevant collective licensing agreements,
no reproduction of any part may take place without
the written permission of Cambridge University Press.

First published 1997

Printed in the United Kingdom at the University Press, Cambridge

A catalogue record for this book is available from the British Library

Library of Congress Cataloguing in Publication data

Nonlinear dynamics, chaotic and complex systems: proceedings of an international conference held in
Zakopane, Poland 7-12, 1995: plenary invited lectures/edited by E. Infeld, R. Żelazny, A. Gałkowski.

p. cm.

ISBN 0 521 58201 6 (hardcover)

1. Differentiable dynamical systems - Congresses. 2. Chaotic behavior in systems - Congresses. 3. Nonlinear
theories - Congresses. I. Infeld, E. (Eryk) II. Żelazny, Roman. III. Gałkowski A. (Andrzej). 1951-

QA614.8 N66 1997

003'.85-dc21 97-4012 CIP

ISBN 0 521 58201 6 hardback

Thermomechanical particle simulations

By W. G. HOOVER¹⁻³, H. A. POSCH¹, CH. DELLAGO¹,
O. KUM^{2,3}, C. G. HOOVER², A. J. DE GROOT^{2,3}
AND B. L. HOLIAN⁴

¹Institut für Experimentalphysik, Universität Wien, Wien, Austria

²Lawrence Livermore National Laboratory, Livermore, USA

³Department of Applied Science, University of California at Davis/Livermore, Livermore, USA

⁴Los Alamos National Laboratory, Los Alamos, USA

Thermomechanics is a generalization of classical mechanics in which heat transfer and temperature play essential roles. It is specially useful away from equilibrium. Here we review thermomechanical particle simulation techniques and their applications, both small-scale and large. We illustrate the impact of thermomechanical methods on irreversible statistical mechanics and on the interpretation of macroscopic irreversible phenomena. Pressing problems for the future are also outlined and discussed.

1. Introduction

To simulate open-system flow processes involving heat transfer and dissipation it is necessary to augment conventional Newtonian mechanics with explicit treatments of temperature and heat reservoirs. In § 2 we review the definition of the ideal-gas temperature, and show that it is appropriate for thermomechanical simulations. In § 3 we use Hamilton's Principle of Least Action to incorporate this definition of temperature, with corresponding temperature controls, into particle-based simulations.

Thermomechanical simulations carried out in this way have already led to a variety of results. On the most fundamental microscopic level, a description of the flow within the many-body phase space, the simulations establish interconnections linking the spectrum of Lyapunov instability exponents to the information dimension of time-reversible multifractal repellers and attractors, and to the rate of external entropy production, all in accord with the Second Law of Thermodynamics. These relationships are discussed generally, and illustrated for many-body field-driven flows, in § 4 and § 5. We then consider, in § 6, these fundamental microscopic concepts for the simplest possible problem, the two-dimensional isokinetic Galton Board. Here, the phase space is relatively simple, so that the multifractal nature of the nonequilibrium phase-space distributions can be visualized completely.

Thermomechanical particle simulations have so far provided not only all the relatively simple properties, such as the equilibrium mechanical and thermal equations of state and the nonequilibrium transport coefficients, but also a quantitative treatment of some of the more complicated macroscopic flow processes, such as plasticity and fracture, for which no satisfactory macroscopic explanation exists. Some recent results are described in § 7.

On the macroscopic level, matter is described in terms of its constitutive properties, rather than in terms of interatomic forces. Because particle methods tend to be unusually stable, they are desirable tools for solving macroscopic problems too. But the microscale time and spatial limitations of atomistic particle methods mean that macroscopic problems require macroscopic particles. For such macroscopic problems, Smooth Particle Applied Mechanics is a useful method with some interesting connections to molecular

dynamics. In § 8 we discuss the application of Smooth Particle Applied Mechanics to the simulation of hydrodynamic instabilities. Finally, we comment on some of the puzzling loose ends awaiting a better understanding in the near future.

2. Temperature far from equilibrium

In equilibrium thermodynamics there are many alternative definitions of temperature. The most familiar are:

(i) the ideal-gas temperature scale defined by the pressure of an equilibrium ideal-gas thermometer,

$$T_{\text{ideal gas}} \equiv \frac{PV}{Nk},$$

where P is the isotropic pressure exerted by an N -particle ideal gas in a volume V ,

(ii) the entropic temperature defined by the isochoric entropy derivative of the internal energy,

$$T_{\text{entropic}} \equiv \left(\frac{\partial E}{\partial S} \right)_V.$$

The lack of a satisfactory definition of entropy far from equilibrium, as well as the relative simplicity of the ideal-gas temperature scale, both suggest that the ideal-gas thermometer be selected to define temperature away from equilibrium. A convincing case for this choice can be based on a detailed calculation, using kinetic theory.

If we consider a heavy particle, with mass M and velocity U , able to collide with representative light ideal-gas particles, of mass m and with velocities $\{u\}$ chosen from the Maxwell-Boltzmann velocity distribution characterizing an equilibrium ideal gas at a fixed temperature T , the average momentum transfer $\langle \Delta(MU) \rangle$ and energy transfer $\langle \Delta(MU^2/2) \rangle$ per collision are simple averages, weighted with the mean speed, $|u - U|$, over the Maxwell-Boltzmann distribution of gas-particle velocities. The results are (i) that the heavy-particle velocity decays exponentially to zero while (ii) the average energy, $\langle MU^2/2 \rangle$, approaches the equilibrium value, $DkT/2$, in D dimensions. The number of collisions required for the velocity and energy changes is of order M/m .

Our theoretical knowledge of dilute-gas behavior is summarized by the Boltzmann Equation, which leads again to these same results for the effects of collisions on the heavy-particle velocity and energy. A one-line derivation of them, given by Salmon (1980), is particularly instructive. He takes the point of view that gas-phase momenta change in such a way as to maximize the Boltzmann entropy. He represents this tendency toward equilibration by introducing a generalized entropic force, defined as a gradient in momentum space and taken in the direction of increasing Boltzmann entropy. The magnitude of the characteristic force is determined by the kinetic temperature T . The time required for the force to become effective defines a collision time, τ . Salmon's simple picture leads to the following *ad hoc* recipe for the entropic force:

$$\left(\frac{dp}{dt} \right)_S \equiv -\frac{mkT}{\tau} \nabla_p \ln \left(\frac{f}{f_{\text{eq}}} \right), \quad f_{\text{eq}} \propto \exp \left(-\frac{p^2}{2mkT} \right),$$

which then gives directly the Fokker-Planck equation for the time evolution the one-particle distribution function:

$$\frac{df}{dt} = -\nabla_p \cdot \left[f \left(\frac{dp}{dt} \right)_S \right] \equiv \frac{1}{\tau} \nabla_p \cdot (pf) + \frac{mkT}{\tau} \nabla_p^2 f.$$

The Fokker-Planck equation is of course nothing other than a weak-collision limit of the Boltzmann equation. But its interpretation as the result of an entropic force is interesting.

This point of view associates a common origin for (i) the decay of the velocity toward zero together with (ii) the diffusive randomizing force of collisions, leading to the equilibrium value of the kinetic temperature.

3. Motion algorithms from Least Action

Gillilan & Wilson (1992) showed that the simplest equilibrium application of the Principle of Least Action to conservative particle dynamics, minimizing the action integral for a trajectory from $-dt$ to $+dt$, gives rise to the familiar Størmer integration algorithm, which we write here explicitly as a set of particle motion equations, one for each degree of freedom:

$$\{x_- - 2x_0 + x_+ = (dt)^2 F_0/m\}.$$

The subscripts indicate the times $\{-dt, 0, +dt\}$. In the variational calculation the end-point coordinates $\{x_-, x_+\}$ are fixed. The set of intermediate coordinates $\{x_0\}$ is then varied to minimize the trapezoidal-rule integration of the Lagrangian. The equilibrium motion algorithm which results, the Størmer algorithm, has been used by generations of scientists for solving Newton's conservative equations of motion. The only technical details required to ensure an efficient simulation are (i) short-ranged forces vanishing linearly at a cutoff, so as not to degrade the second-order integrator accuracy, and (ii) a linked-list catalog of near neighbors, so as to make the simulation time proportional to N rather than to N^2 .

The equilibrium Størmer algorithm is patently time-reversible. Levesque & Verlet (1993) pointed out that this reversibility is exact, to the very last bit, provided that the algorithm is applied in an *integer* state space, with all coordinates $\{x(ndt)\}$ integers and with the coordinate changes due to the forces rounded off to integers also. There is very likely no way to apply this idea of exact 'bit reversibility' away from equilibrium.

The least action principle itself *can* be applied away from equilibrium, where it is necessary to control the temperature, or the internal energy, or other dynamical variables. Consider the simplest case, temperature control. To keep the kinetic temperature fixed during the time interval from $-dt$ to $+dt$ requires a Lagrange multiplier to impose the constraint $dK/dt = 0$. The resulting equations of motion:

$$\left\{ \frac{dp}{dt} = F - \zeta_K p \right\}, \quad \zeta_K = -\frac{1}{2K} \frac{dE}{dt},$$

can be solved with a slight modification of the Størmer algorithm or, if better accuracy is desired, by using a conventional fourth-order Runge-Kutta integrator.

It is noteworthy that these isokinetic equations of motion are still time-reversible. In the reversed motion both the momenta $\{p\}$ and any friction coefficients $\{\zeta_K\}$ change sign. It is straightforward to generalize the least-action derivation of the motion algorithm to treat time-dependent constraints or to constrain the internal energy in the presence of external fields. We explore both the constrained and unconstrained algorithms in the two following sections.

4. Conservative nonequilibrium simulations

The difficulties involved in simulating nonequilibrium flows with Newtonian mechanics can best be appreciated by considering a simple example, a fluid in which half the particles are accelerated to the right, and half to the left, by an external field of fixed strength F . We choose to study a two-dimensional square 36-particle system of particles interacting

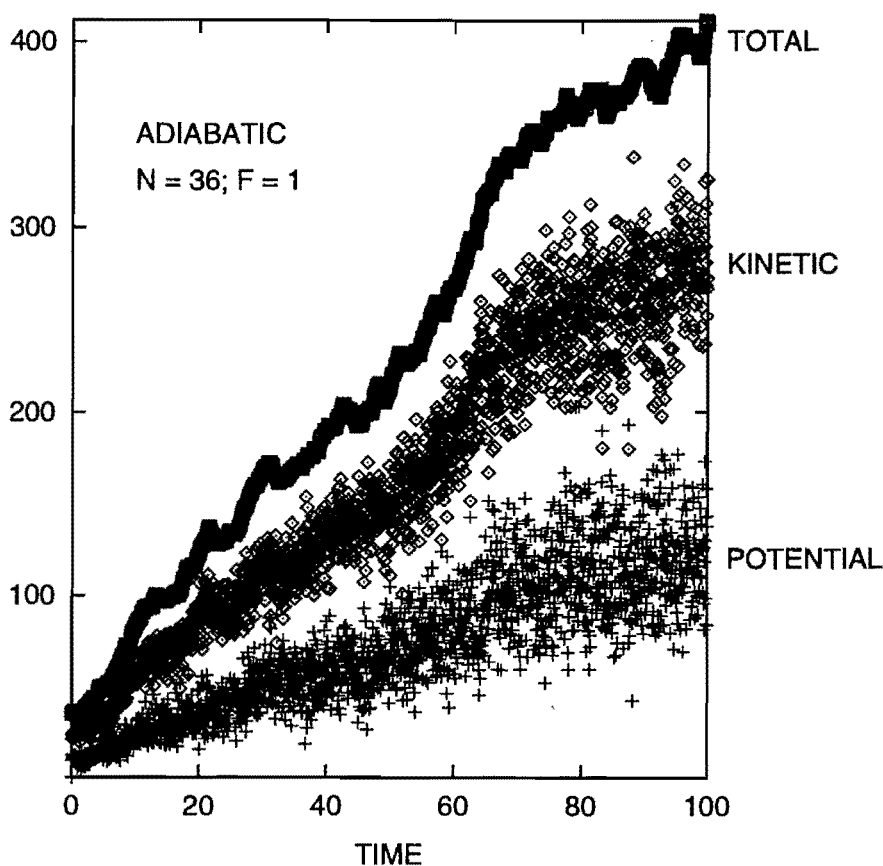


FIGURE 1. Time variation of the total, kinetic, and potential energies for a system of 36 particles driven by a field of unit strength. The mechanics is purely Hamiltonian, so that the system heats up with no increase in phase volume.

with a short-ranged repulsive potential,

$$\phi = 100 \epsilon [1 - (r/\sigma)^2]^4.$$

The overall reduced density is unity, so that $V = N\sigma^2$. For convenience we choose reduced units with the energy ϵ , the collision diameter σ , and the particle mass m all set equal to unity. We further choose the forces due to the external field F equal to $\{(\pm 1, 0)\}$.

With the periodic boundaries usual in simulations of bulk properties, intuition, bolstered by the numerical results shown in figure 1, suggests that such a field-driven system has no nonequilibrium steady state. If the field is reasonably strong, currents develop and the system heats up. The rate at which work is done by the field, $F \cdot JV$, where J is the current density, then causes a proportional heating of the fluid. As the fluid heats up, the heating effect of the field becomes relatively less important, until, at sufficiently high temperature, the motion more and more closely approximates that of an equilibrium system. Evidently such an adiabatically heated system never achieves a steady state and instead only proceeds, with gradually increasing fluctuations, in the general direction of equilibrium.

It is interesting to see that, even with a very strong external field, the resulting nonequi-

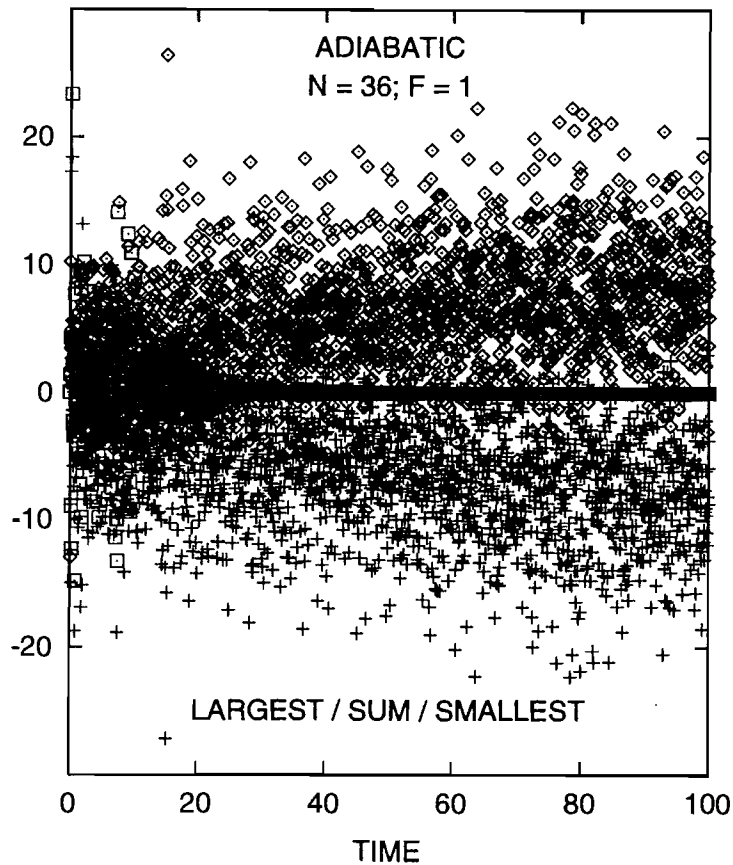


FIGURE 2. Time variation of the largest and smallest local Lyapunov exponents in the 36-particle adiabatic simulation of figure 1. The sum of the local exponents is also plotted, and shows that the instantaneous values become paired, following the decay of transients, at a reduced time of approximately 40.

librium motion remains adiabatic and its phase-space description is straightforward. Such a phase-space flow obeys Liouville's Theorem, taking place at constant phase volume. Thus, if we imagine the motion of a small phase-space hypervolume surrounding our trajectory's initial state, the density associated with that volume is carried along forever, without change. Figure 1 shows the increase of energy and temperature for a reduced time of 100. Figure 2 shows the pairing of the local (instantaneous) Lyapunov exponents that occurs, as it must for any solution of Hamilton's equations of motion. The vanishing of the summed exponents shows that there is no change in the comoving phase-space volume.

This example, like the more familiar free-expansion one, shows the inadequacy of Gibbs' statistical entropy away from equilibrium. Entropy, unlike pressure and temperature, has no mechanical analog, and so is not a useful concept far from equilibrium. There is no analog of Zermélo's Recurrence Paradox here because the periodic boundaries make energy a multiple-valued function of the particle coordinates. The Lyapunov spectrum for such a time-reversible flow, two exponents for each degree of freedom, is

composed of rapidly fluctuating Smale pairs which individually sum to zero, as shown, for one pair, in figure 2.

There are only two ways to compute averaged quantities, as dynamical time averages or as statistical phase averages. *At equilibrium* either approach can be followed. Although time averages are certainly more closely linked to experiments, the availability of Gibbs' equilibrium distributions makes phase averages nearly as attractive. *Away from equilibrium* the situation is very different. The phase-space distribution is multifractal and is *never* known in advance. It can only be determined through dynamical simulation. Thus, away from equilibrium, the simplest, and most informative, approach is to analyze a single long trajectory generated by special steady-state boundary conditions. We illustrate this approach in the following section.

5. Reversible dissipative nonequilibrium simulations

In his stimulating lectures *On the Character of Physical Law*, Feynman repeatedly emphasized the fundamental nature of Hamilton's Principle of Least Action. We have seen that this principle provides a basis for the most commonly used conservative integration algorithm. Exactly the same approach can also be successful in the nonequilibrium case, where thermostats, or ergostats, or barostats need to be used to induce a nonequilibrium steady state. With such constraint forces field-driven heating no longer leads to an unsteady state. Instead the motion converges to a nonequilibrium steady state. Under such constrained conditions, the Lyapunov spectrum is no longer symmetric, though a modified Smale pairing of the time-averaged exponents can persist. Sarman *et al.* (1992) established the conditions under which 'conjugate pairs' of exponents undergo identical shifts.

In phase space the motion collapses onto a multifractal strange attractor. The information dimension of this attractor is the dimensionality of the largest comoving phase-space object which does not get smaller as time goes on. As Kaplan and Yorke suggested, it can be estimated from the Lyapunov spectrum by finding the maximum number of exponents which can be summed, with the sum remaining positive. In the case of field-driven currents the numerical results indicate an information dimension which decreases below the equilibrium value in proportion to the square of the field strength.

To achieve an isoenergetic steady state, the equations of motion derived from the Least Action Principle are the following:

$$\left\{ \frac{dp}{dt} = -\nabla\Phi \pm F - \zeta_E p \right\}, \quad \zeta_E = \sum \frac{\pm F \cdot p}{2mK}.$$

Figure 3 shows results for the same 36-particle field-driven system discussed earlier, but with an isoenergetic constraint imposed for reduced times greater than 50. The kinetic and potential energies continue to fluctuate normally. The instantaneous values of the largest and smallest Lyapunov exponents, and their sum, is shown in figure 4. Though Sarman *et al.* (1992) showed that the pairing rule must be satisfied for the global averaged exponent pairs, a close examination of the data here show that there is no exact pairing for the local exponents. Considerably larger deviations from instantaneous pairing occur if an isokinetic, rather than isoenergetic, constraint is imposed. In either constrained nonequilibrium case the overall sum of the global exponents is negative, reflecting the collapse of the comoving phase volume onto a strange attractor. This collapse, which is qualitatively unlike the adiabatic constant-volume flow, corresponds to a steady divergence of the Gibbs entropy, which approaches $-\infty$ at long times.

The special time-reversible equations of motion used here have interesting consequences

ro, as shown,
 ti averages
 followed. Al-
 availability of
 e. *Away from*
 s multifractal
 ical simula-
 approach is to
 ry conditions.

peatedly em-
 We have seen
 ve integration
 ilibrium case,
 a nonequilib-
 ger leads to an
 state. Under
 tric, though a
 n *et al.* (1992)
 lergo identical

. The informa-
 ng phase-space
 e s rested, it
 m. of expo-
 of field-driven
 ecreases below

from the Least

cussed earlier,
 than 50. The
 taneous values
 wn in figure 4.
 d for the global
 at there is no
 instantaneous
 osed. In either
 its is negative,
 ttractor. This
 corresponds to
 times.
 g consequences

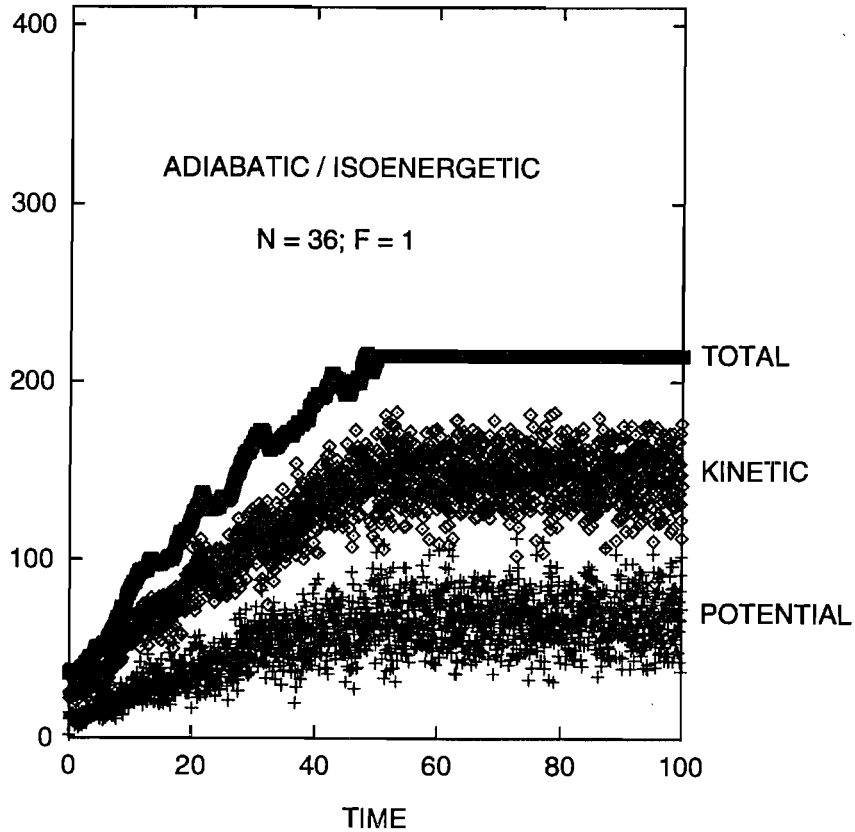


FIGURE 3. Time variation of the total, kinetic, and potential energies for a system of 36 particles driven by a field of unit strength. The total energy is constrained, and the comoving phase volume begins to collapse to a strange attractor, at a reduced time of 50.

for the phase-space flow. Liouville's Theorem for the flow establishes that the constrained comoving phase volume changes with time according to the instantaneous values(s) of the friction coefficient(s):

$$\frac{d \ln f}{dt} \equiv \sum \zeta_E,$$

where the sum includes all ergostatted degrees of freedom. Conservation of the comoving phase-space probability, $f \otimes$, where \otimes is the small comoving element of phase volume, occupied by f , relates the sum of Lyapunov exponents to the sum of the friction coefficients:

$$\sum \lambda \equiv \left\langle \frac{d \ln \otimes}{dt} \right\rangle \equiv \left\langle -\frac{d \ln f}{dt} \right\rangle = \left\langle -\sum \zeta_E \right\rangle,$$

where the angular brackets $\langle \cdot \rangle$ indicate a time average. Finally, the external heat exchanged through the friction coefficients, divided by the temperature of the exchange, gives the rate of external entropy production, dS/dt . As a direct consequence of the least-action approach to deterministic temperature and heat transfer there results the exact chain of relations linking the *instantaneous* friction coefficients, the *instantaneous*

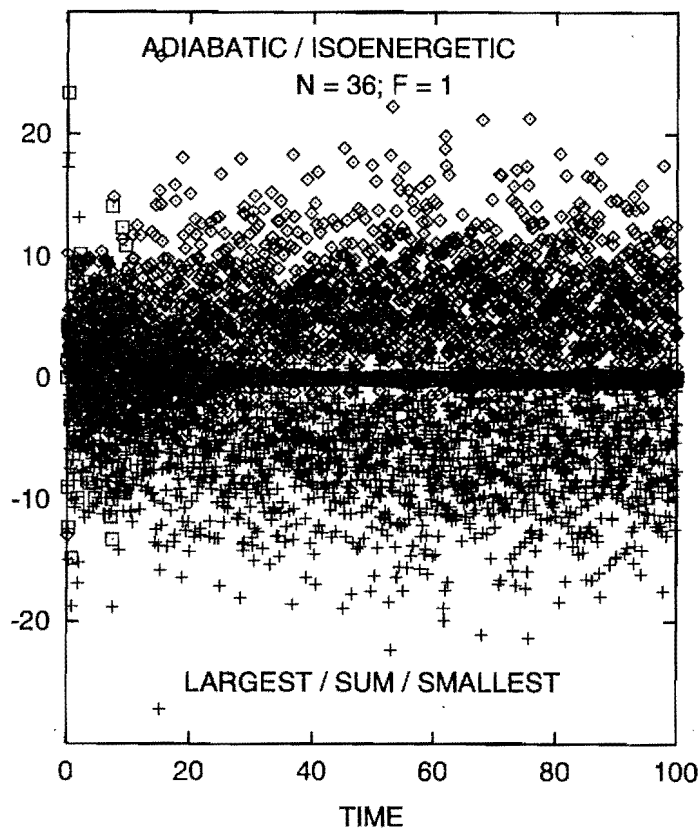


FIGURE 4. Time variation of the largest and smallest local Lyapunov exponents in the 36-particle constrained isoenergetic simulation of figure 2. In this case the exact instantaneous pairing of pairs of exponents is destroyed by the isoenergetic constraint.

Lyapunov exponents, and the *instantaneous* entropy production:

$$\sum \zeta_E \equiv - \sum \lambda \equiv \frac{d(S/k)}{dt}.$$

Of course, this chain of instantaneous equalities applies just as well to the time-averaged quantities.

The qualitative phenomenon illustrated here, the breaking of the symmetry of the Lyapunov spectrum, with the summed spectrum reproducing the rate of external entropy production, is a perfectly general consequence of the time-reversible equations of motion based on the Principle of Least Action. Because the geometric features associated with irreversibility are much more easily demonstrated in small systems, we consider the two-body version of this nonequilibrium problem in the next section.

6. Quantitative results from the Galton board

Historically, the Galton Board was the first system for which the generic multifractal time-reversible phase-space structure just discussed was established, see Machta & Zwanzig (1983), Ladd & Hoover (1985), Hoover *et al.* (1985), Moran *et al.* (1987), Hoover *et al.* (1988), Hoover & Moran (1989), Hoover & Moran (1992), Vance (1992), Hoo-

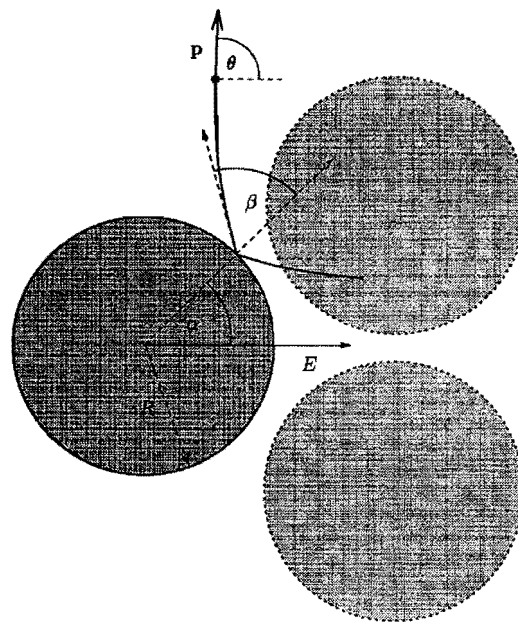


FIGURE 5. Definition of the angles α and β defining a hard-disk collision in the Galton Board. θ gives the direction of the particle velocity relative to the field direction.

ver *et al.* (1992), Chernov *et al.* (1993), Petracic *et al.* (1994), Lloyd *et al.* (1995) and Dellago *et al.*. The first nonequilibrium simulations, see Machta & Zwanzig (1983), incorporated shear, and were a caricature of viscous flow. By 1985, studies of field-driven diffusion became more common than studies of shear, mainly because diffusion is a slightly simpler problem, with fewer phase-space dimensions. These two viscous and diffusive Galton Board models are representative of the computer revolution in physics, in which models are chosen for study because they are both instructive and computationally feasible, though not necessarily analytically tractable. Thus the Galton Board is more informative than is the Baker Map though the Baker Map is more easily analyzed. The Galton Board occupies an interesting middle ground in which many of the results established numerically could also be deduced from a purely theoretical basis. Such a model is very useful for the progress of mathematical physics. Simulations stimulate theoretical advances which then feed back new ideas for simulation. That the Galton Board has been specially fruitful for nonequilibrium statistical mechanics is clear from the references cited by Dellago *et al.* (1995).

The Galton Board problem is a special two-body version of the simple field-driven constrained problem of the last section. The periodic boundaries are chosen to be consistent with a particular lattice structure, here the triangular lattice, and the driving field is chosen in a particular direction, here perpendicular to one of the three directions of closest packing. To simplify the dynamics, the interparticle interaction is further simplified to an impulsive hard-disk interaction. The field-dependent conductivity is defined in the usual way, as the ratio of the current to the field strength. Though the problem is at first glance complicated, being described by eight phase-space variables, $\{x, y, p_x, p_y\}$, fixing the center of mass and the kinetic energy gives five constraints, so that the motion occurs in a three-dimensional phase space. The description can be further simplified, reducing

30 title
paving of

averaged

try of the
al entropy
of motion
iated with
r the two-

multifrac-
Machta &
987), Hoo-
992), Hoo-

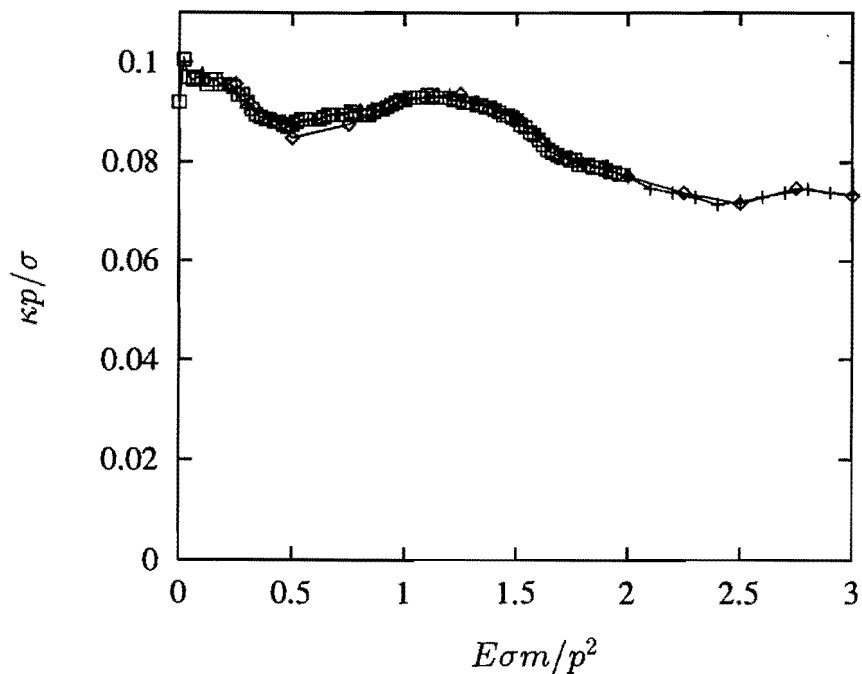


FIGURE 6. Variation of Galton Board conductivity as a function of field strength at 4/5 the close-packed density. The points shown are taken from Moran *et al.* (1987), Dellago *et al.* (1995) and Lloyd *et al.* (1995). The agreement among these three data sets is excellent.

to a list of successive collisions, each of which can be described by two angles, α and β , as defined in figure 5.

The conductivity and the phase-space densities for this model were known in 1986. The Lyapunov exponents have just very recently been calculated. There are only two, with the sum negative, equal to the rate at which field energy is dissipated by the ergostat. The variation of the conductivity, Lyapunov exponents, and a Poincaré section of the phase-space density with field strength are shown in the figures 6–8. The multifractal phase-space structure, with an information dimension strictly less than the equilibrium value, and the positive transport coefficient, despite time-reversible equations of motion, are both characteristic of all nonequilibrium simulations employing time-reversible thermostats or ergostats. The Galton Board is the first model for which these results were established, both numerically and theoretically.

It is noteworthy that the time-reversed attractor is the unstable phase-space repeller, on which the Second Law of Thermodynamics is violated. Because this repeller has a space-filling ergodic character, with Hausdorff dimension equal to the embedding dimension, there is a repeller point arbitrarily close to any point in space. Thus this chaos could easily be 'controlled' to get a current violating the Second Law by converting heat to work.

7. Microscopic plasticity and fracture simulations

Atomistic simulations of the progress of dislocations and cracks through crystals have been carried out for 20 years. These simulations are motivated by the failure of continuum

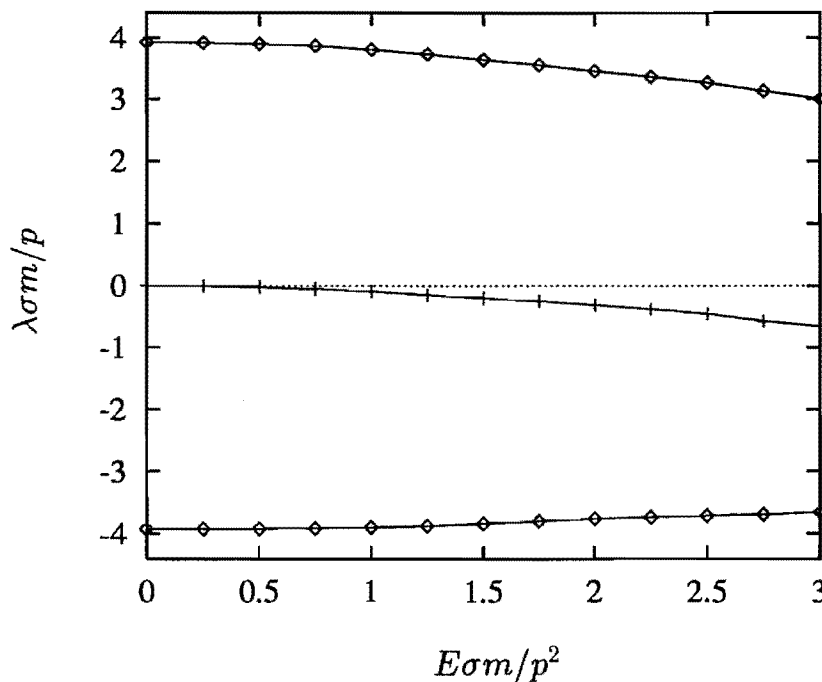


FIGURE 7. Variation of Galton Board Lyapunov exponents as a function of field strength at $4/5$ the close-packed density. The sum of the exponents is also plotted and is equal to $-d(S_{\text{external}}/k)/dt$.

mechanics to deal satisfactorily with atomic-scale failure processes. Of course, the forces used in the atomistic simulations are oversimplified and speculative, so that neither a microscopic nor a macroscopic picture can provide a quantitative understanding of 'real' plasticity and fracture. The embedded-atom potential provides the necessary flexibility for dealing with metals, which are only poorly described by pair potentials.

Some of the largest-scale molecular dynamics simulations to date, with more than ten million particles, have been carried out at Los Alamos. Goals of this work are, first, to characterize both brittle and ductile crack growth and bifurcation, and then, to understand the influences of temperature and interparticle forces on these features. Figure 9 shows a bifurcated crack, propagating through a cold two-dimensional crystal of a quarter million atoms. To prevent sound waves from reflecting at the system boundaries, special viscoelastic boundaries were developed and implemented in regions with a width of twenty atomic diameters.

The first large-scale nonequilibrium simulations of plastic flow in three dimensions were devoted to the deformation of models of crystalline and amorphous silicon. Apart from the complexity of dealing with three-body forces, the main problem involved developing boundary conditions describing the interaction of an indenter with the silicon workpiece. Eventually these plasticity simulations were carried out with over a million atoms, and at sufficiently low deformation rates to provide a size-independent yield strength in accord with experiment. A specimen simulation is shown in figure 10. Such simulations revealed both a shear-induced phase transformation and the formation mechanism for new surfaces adjacent to the indenter. Both the fracture and plasticity simulations would have been

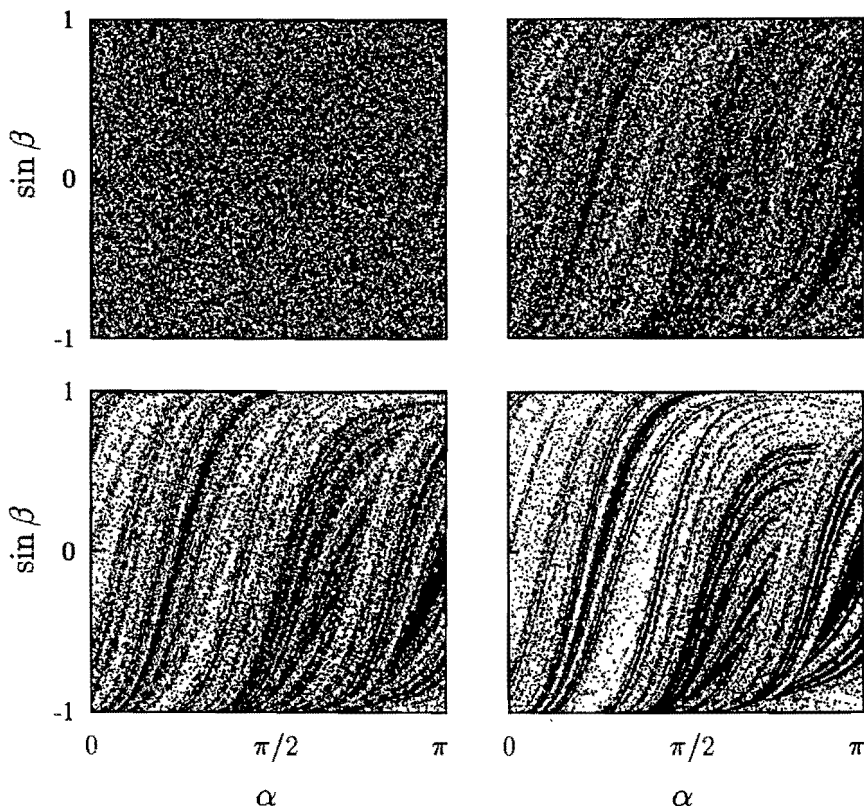


FIGURE 8. Typical phase-space sections showing the distribution of collisions as a function of field strength, all at $4/5$ the close-packed density. The field strengths shown are 0, 1, 2, and 3, in units of $p^2/(m\sigma)$, where a point mass m , with momentum p , is scattered by disks of diameter σ .

impossibly time-consuming ten years ago. Both required parallel processors, linked lists of neighbors, and special boundary conditions for extracting energy and momentum from the system.

8. Smooth Particle Applied Mechanics

Particle methods can be applied to macroscopic problems too, using Smooth Particle Applied Mechanics, a technique invented by Lucy and Monaghan in 1977, see Lucy (1977) and Monaghan (1992). The individual smooth particles represent smoothed distributions of material, with their own masses, energies, velocities, stresses, heat fluxes, etc. The mass distribution of each particle in space is described by a weighting function $w(r)$ which is usually, but not invariably, fixed in form and range. Typically, the first and second derivatives of $w(r < h)$ vanish at the cutoff radius, h , which is chosen sufficiently large that each particle interacts with thirty or forty others. Values of the various continuum flow variables are obtained as sums of particle contributions. Density is an important example. The density at a location r is calculated as a sum of contributions from the



π

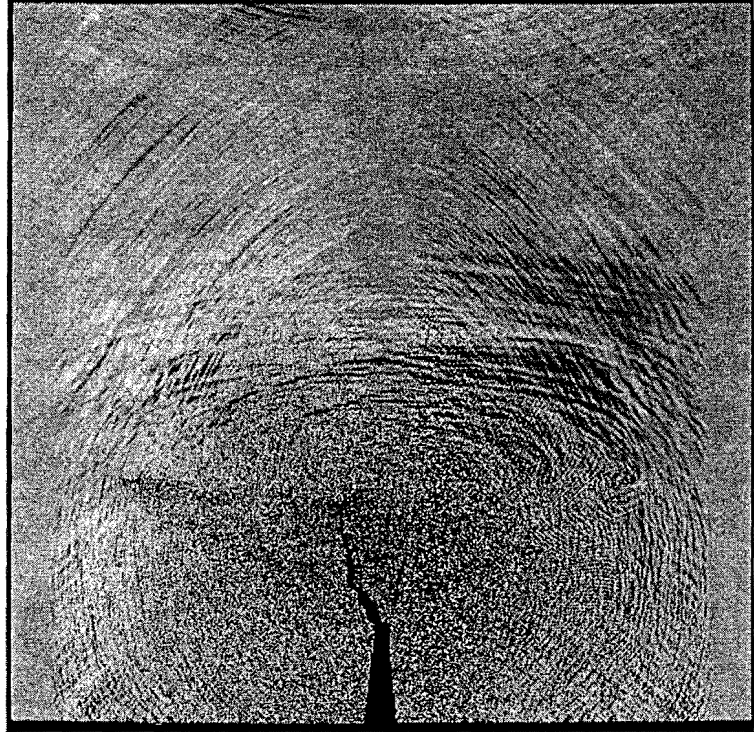


FIGURE 9. Propagation of a crack through a cold two-dimensional crystal of Lennard-Jones particles with quiet boundaries. Note the bifurcation, or branching of the crack. The vertical boundaries contain particles interacting with dashpot forces which increase in strength over a region twenty atomic diameters in width.

function of
1, 2, and 3,
of the center

weights of all nearby smooth particles:

$$\rho(r) \equiv \sum m w(r - r_i),$$

This simple formulation makes it unnecessary to solve the continuity equation.

The motion equations for the smooth particles involve the individual stresses as the gradients of the weighting, or smoothing, functions which describe the positions of the particles in space:

$$\left\{ \frac{dv_i}{dt} = \sum m [(\sigma/\rho^2)_i + (\sigma/\rho^2)_j] \cdot \nabla_i w_{ij} \right\}.$$

To the extent that the stress and density are slowly varying in space, the smooth-particle trajectories look just like particle trajectories governed by a pair potential proportional to $w(r)$.

Smooth particles have mostly been used to solve difficult problems in astrophysics, but there are beginning to be more applications to familiar problems in fluid mechanics. Figure 11 shows a single frame from a two-dimensional smooth-particle simulation of the Rayleigh-Bénard instability, the formation of convective rolls when an expanding fluid is exposed, simultaneously, to a temperature gradient and a gravitational field. A detailed investigation shows that systems of a few thousand particles are sufficient to reproduce the kinetic energy and the time development of the instability.

linked lists
entrum from

with Particle
Jucy (1977)
distributions
, etc. The
 $w(r)$ which
and second
iently large
continuum
important
is from the

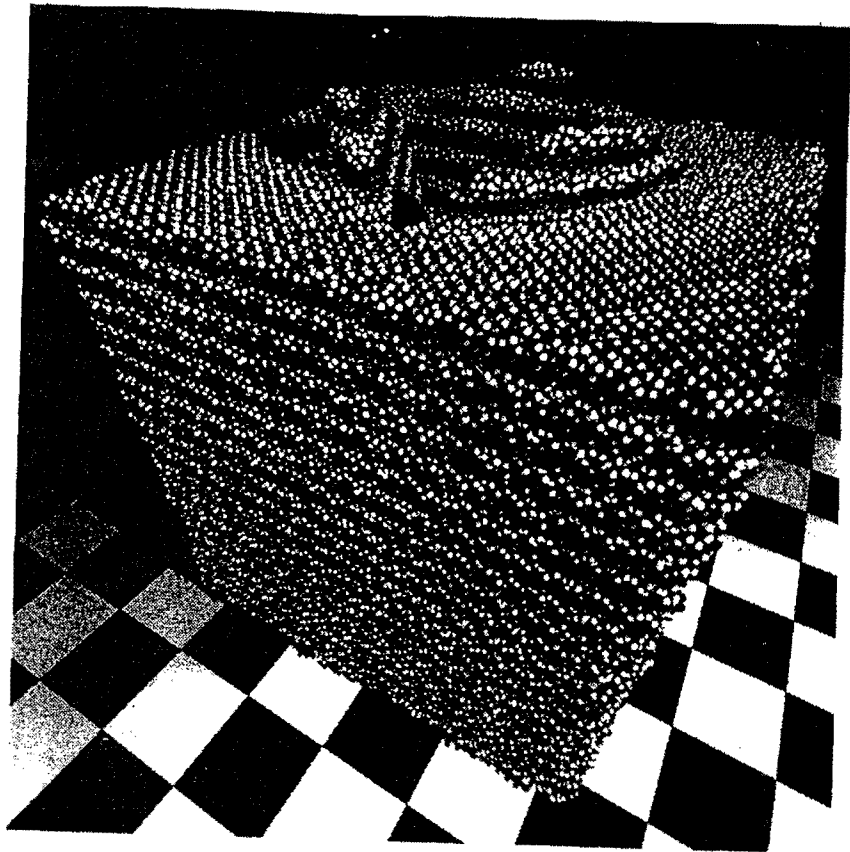


FIGURE 10. Indentation pit in a model of silicon. The tetrahedral indenter which created the pit moved at $1/5$ the speed of sound. The simulation shown here used 373,248 silicon atoms.

the exact continuum flow field within a few percent, see Rapaport (1988), Puhl *et al.* (1989), Posch *et al.* (1995) and Kum & Hoover (1995). Figure 12 compares density and temperature contours calculated with 5000 smooth particles with exact contours obtained from a grid-based solution of the Navier–Stokes equations.

The similarity of the smooth particle motion equations to the microscopic ones makes smooth particles a promising component of hybrid models spanning a range of space and time scales. In solutions of the continuum equations, boundary conditions often present a major difficulty. In the smooth particle case, two different types of boundaries have proved very useful. Mirror boundaries, shown in figure 11, associate image particles with those bulk particles within range of the boundary. An explicit treatment of surfaces, based on a smooth particle analog of surface tension, has proved useful for simulating both static and rotating liquid drops and for studying the instability of the interface between materials of differing densities.

The accurate treatment of material surfaces is a research frontier in numerical continuum mechanics. In simulations of automobile collisions or the unstable buckling of structures composed of struts, it is essential to find all material contacts in a complex mesh, quickly and reliably. This can be done by using a generalization of the linked-list approach, with an additional space-fixed grid devoted to the detection and prevention

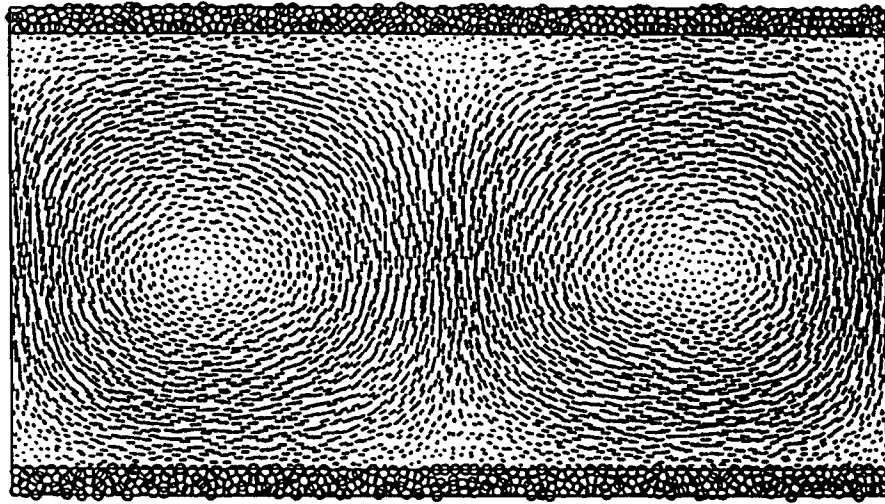


FIGURE 11. Typical smooth-particle velocity distribution for Rayleigh-Bénard flow; 5000 smooth particles were used. Note the reflected image particles at the top and bottom boundaries.

11.5
4.5

of intersurface contacts. Figure 13 shows the deformation of a sheet made up of elastic-plastic shell elements. The sheet was crumpled, to form a wad, by simultaneously squeezing the original structure between three pairs of mutually-orthogonal moving plane walls. The resulting structure has several interesting multifractal aspects.

9. Puzzles for the future

One of the stated goals of the conference organizers is to identify current problems important for the future growth of understanding and applying Chaotic Complex Systems. From the perspective of particle simulations there are several areas which need more attention. In outline form these are

- (i) characterizing multifractal objects,
- (ii) understanding ergodic strange attractors,
- (iii) developing smooth boundaries,
- (iv) excluding unwanted fluctuations,
- (v) improving our description of turbulence,
- (vi) relating Nosé's mechanics to mechanical variational principles.

Let us consider each of these problem areas in more detail.

The most basic need is for better characterization of the fractal objects themselves. For these objects, the fractal dimension, or dimensions, or its spectrum, are not sufficiently detailed to distinguish a crumpled sheet of paper from a puffy cumulus cloud. More quantifiable descriptors of fractal geometry are sorely needed to help us find our way around in the zoo of these objects.

The fractal objects generated by nonequilibrium particle simulations are mathematically subtle. It seems evident that the twin notions of (a) ubiquitous shrinking of phase volume onto a strange attractor which is simultaneously (b) ergodic are dangerously close to nonsense. For an integer (or rational) state space these two things cannot both be true.

6.6

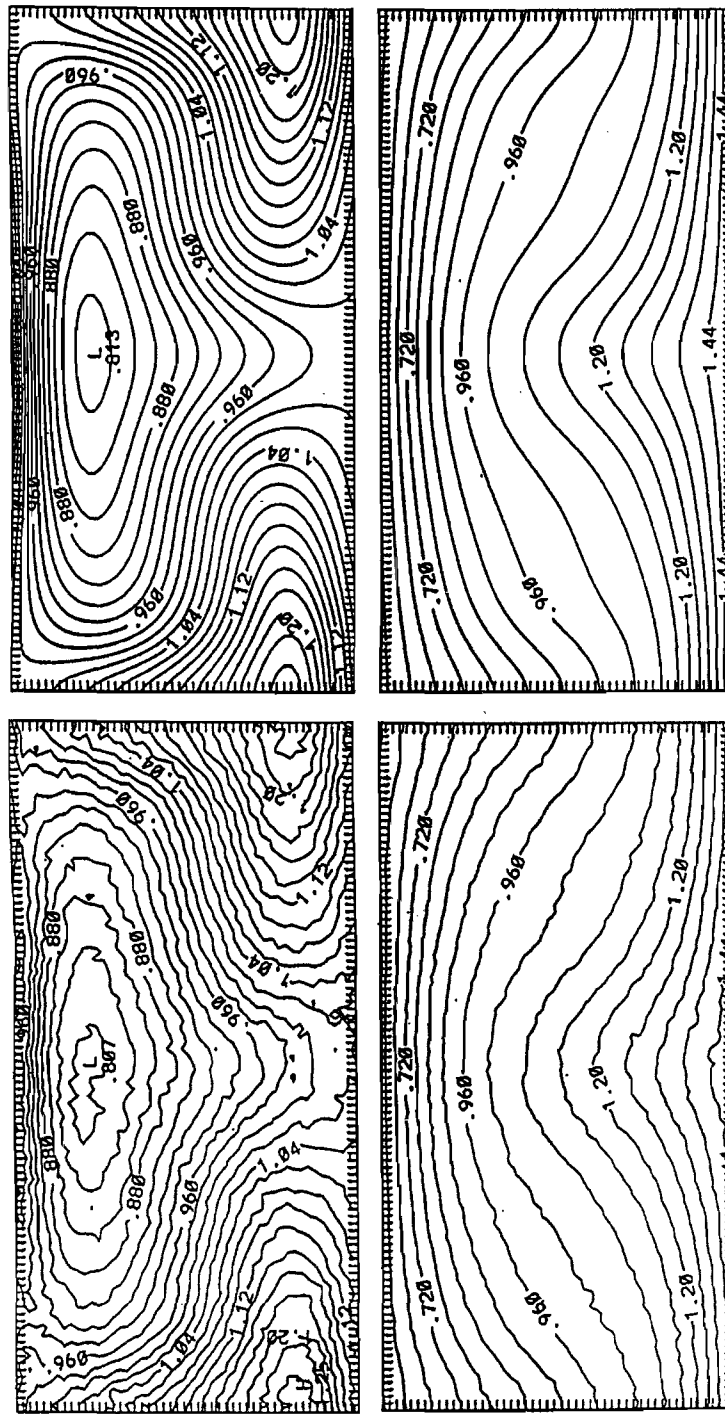


FIGURE 12. Density and temperature profiles for the smooth-particle simulation of figure 11 are compared to exact profiles from a highly-accurate solution of the continuum equations.

67

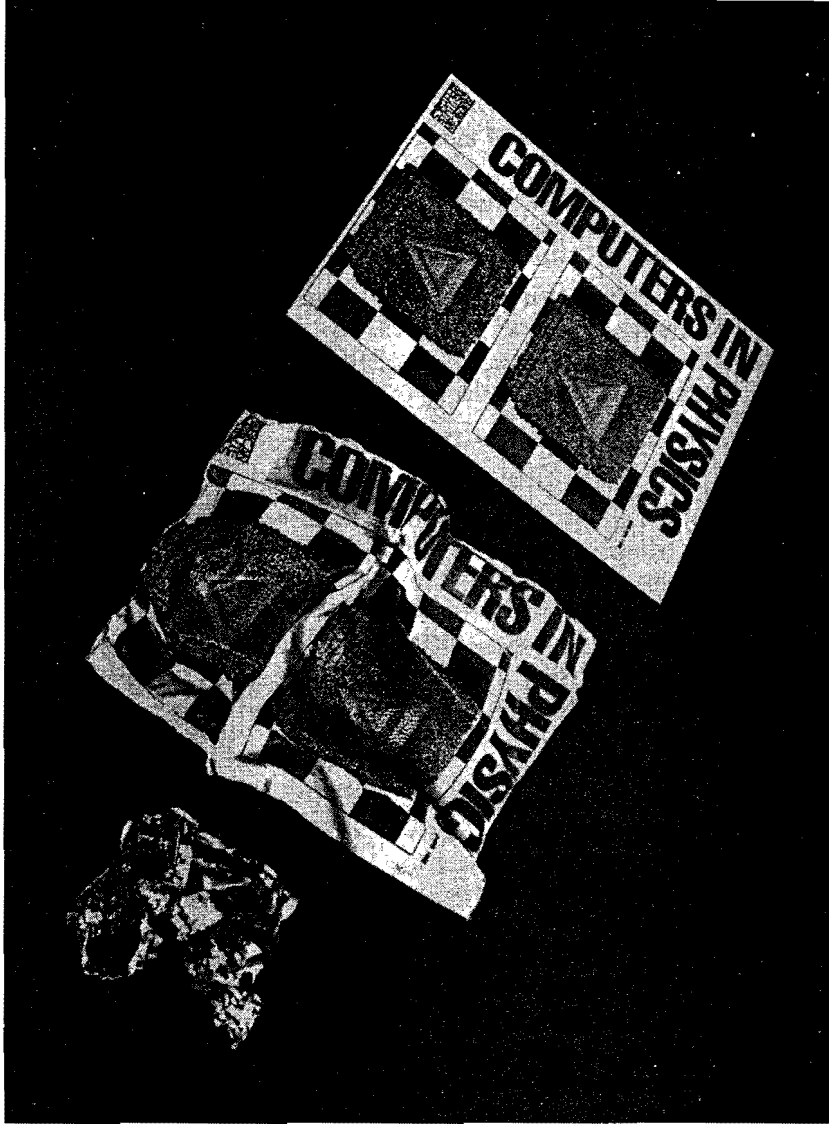


FIGURE 13. Simulation of the crumpling of a structure composed of elastic-plastic elements using the computer program DYNA3D.

Nevertheless, the shrinkage in phase space and the ergodicity are both characteristic of the fractal objects of most interest for physicists.

The simultaneous shrinking and recurrence bring to mind some paradoxical mathematics from two generations ago. The Banach-Tarski paradox refers to that deep set theory, when augmented by the Axiom of Choice, which makes it possible to assemble two identical objects from the cut-up pieces of another. This paradox has been nicely illustrated, using oranges, by French (1988). This failure of augmented set theory to conserve mass is likely related to our present conceptual difficulties in understanding multifractal objects.

Other immediate needs of particle simulators are more special and have to do with smooth and quiet boundaries, the number of degrees of freedom, and fluctuations. Simulation boundaries need to be made as smooth as is possible. An atomistic adaptation of the smooth-particle image approach might be useful. It is also desirable to reduce the number of extraneous degrees of freedom. All particle models are saddled with fluctuations (called 'heat', in the case of molecular dynamics) which can be both realistic and interesting, but with a cost which greatly exceeds their benefit. A means of discarding irrelevant degrees of freedom would be welcome. Finding an efficient route to the Kolmogorov spectrum of turbulence using smooth particles is a related interesting open problem.

For simplicity we have discussed here only isoenergetic and isokinetic forms of equilibrium and nonequilibrium mechanics. Nosé (1991) discovered a generalization of mechanics, designed to replicate Gibbs' canonical distribution in the equilibrium case, now called Nosé-Hoover mechanics. So far the link of that mechanics to the variational principles is missing.

WGH thanks the Universities of California and Vienna, as well as the organizers of this meeting, for making it possible to present this work at Zakopane. Work at the Lawrence Livermore National Laboratory and at the Los Alamos National Laboratory was performed under the auspices of the United States Department of Energy, according to Contracts W-7405-Eng-48 and W-7405-Eng-36. Work at the University of Vienna was supported by the Fonds zur Förderung der Wissenschaftlichen Forschung, Grant P9677. Though this paper primarily reflects the views of WGH and HAP, it was made possible by the dedicated work of all the authors.

REFERENCES

- CHERNOV, N. I., EYINK, G. L., LEBOWITZ, J. L. & SINAI, Y. G. 1993 Derivation of Ohm's law and a deterministic mechanical model. *Phys. Rev. Letts.* **70**, 2209. The reader is cautioned that the multifractal dimension referred to in this reference as a 'Hausdorff dimension' is more often referred to as the 'information dimension'.
- DELLAGO, C., GLATZ, L. & POSCH, H. A. 1995 *Phys. Rev. E* **52**, 4817.
- FRENCH, R. M. 1988 *Mathematical Intelligencer* **10**(4), 21.
- GILLILAN, R. E. & WILSON, K. R. 1992 *J. Chem. Phys.* **97**, 1757.
- HOOVER, W. G. 1992 In *Microscopic Simulations of Complex Hydrodynamic Phenomena* (ed. M. Mareschal & B. L. Holian). Plenum. See particularly figure 4.
- HOOVER, W. G. & MORAN, B. 1989 *Phys. Rev. A* **40**, 5319.
- HOOVER, W. G. & MORAN, B. 1992 *Chaos* **2**, 599.
- HOOVER, W. G., MORAN, B., HOOVER, C. G. & EVANS, W. J. 1988 *Phys. Lett. A* **133**, 114.
- HOOVER, W. G., WINER, K. A. & LADD, A. J. C. 1985 *Intl. J. Eng. Sci.* **23**, 483.
- KUM, O., HOOVER, W. G., & POSCH, H. A. 1995 *Phys. Rev. E* **52**, 4899.
- LADD, A. J. C. & HOOVER, W. G. 1985 *J. Stat. Phys.* **38**, 973.
- LEVESQUE, D. & VERLET, L. 1993 *J. Stat. Phys.* **72**, 519.
- LLOYD, J., NIEMEYER, M., RONDONI, L. & MORRISS, G. P. 1995 *Chaos* **5**, 536.
- LUCY, L. B. 1977 *Astron. J.* **82**, 1013.
- MACHTA, J. & ZWANZIG, R. W. 1983 *Phys. Rev. Letts.* **50**, 1959.
- MONAGHAN, J. J. 1992 *Ann. Rev. Astron. & Astrophys.* **30**, 543.
- MORAN, B., HOOVER, W. G. & BESTIALE, S. 1987 *J. Stat. Phys.* **48**, 709.
- NOSÉ, S. 1991 *Prog. Theor. Phys. Suppl.* **103**, 1.

- PETRAVIC, J., ISBISTER, D. J. & MORRIS, G. P. 1994 *J. Stat. Phys.* **76**, 1045.
 POSCH, H. A., HOOVER, W. G., & KUM, O. 1995 *Phys. Rev. E* **52**, 1711.
 PUHL, A., MANSOUR, M. M. & MARESCHAL, M. 1989 *Phys. Rev. A* **40**, 1999.
 RAPAPORT, D. C. 1988 *Phys. Rev. Lett.* **60**, 2480.
 SALMON, J. 1980 *Hadronic Journal* **3**, 1080.
 SARMAN, S., EVANS, D. J. & MORRIS, G. D. 1992 *Phys. Rev. A* **45**, 2233.
 VANCE, W. N. 1992 *Phys. Rev. Lett.* **69**, 1356.

See also (numerals in parantheses following references indicate related sections):

- ABRAHAM, F. F., BRODBECK, D., RAFEY, R. A. & RUDGE, W. E. 1994 *Phys. Rev. Lett.* **73**, 272. (7).
 ASHURST, W. T. & HOOVER, W. G. 1976 *Phys. Rev. B* **14**, 1465. (7).
 BERENDSEN, H. J. C. & VAN GUNSTEREN, W. F. 1986 In *Molecular-Dynamics Simulation of Statistical-Mechanical Systems* (ed. G. Ciccotti & W.G. Hoover). North-Holland. (2,3).
 FOILES, S. M., BASKES, M. I. & DAW, M. S. 1986 *Phys. Rev. B* **33**, 7982. (2,3).
 GRAY, S. K., NOID, D. W. & SUMPTER, B. G. 1994 *J. Chem. Phys.* **101**, 4062. (2,3).
 HOLIAN, B. L., DE GROOT, A. J., HOOVER, W. G. & HOOVER, C. G. 1990 *Phys. Rev. A* **41**, 4552. (2,3).
 HOLIAN, B. L., HOOVER, W. G., & POSCH, H. A. 1987 *Phys. Rev. Letts.* **59**, 10. (6).
 HOLIAN, B. L. & RAVELO, R. 1995 *Phys. Rev. B* **51**, 11275. (7).
 HOLIAN, K. S. & HOLIAN, B. L. 1989 *Intl. J. Impact Eng.* **8**, 115. (7).
 HOOVER, W. G. 1988 Reversible mechanics and time's arrow. *Phys. Rev. A* **37**, 252. This paper was written for a special issue of the Journal of Statistical Physics, honoring Professor Prigogine (September, 1987), but was rejected. (5,6).
 HOOVER, W. G. 1993 *Physica A* **194**, 450. (6).
 HOOVER, W. G. 1995 *Phys. Letts. A* **204**, 133. (2,3).
 HOOVER, W. G., HOLIAN, B. L. & POSCH, H. A. 1993 *Phys. Rev. E* **48**, 3196. (2,3).
 HOOVER, W. G. & POSCH, H. A. 1994 *Phys. Rev. E* **49**, 1913. (6).
 HOOVER, W. G., POSCH, H. A., HOLIAN, B. L., GILLAN, M. J., MARESCHAL, M. & MASSOBRIO, C. 1987 *Mol. Sim.* **1**, 79. (6).
 KUSNEZOV, D., BULGAC, A. & BAUER, W. 1990 *Annals of Physics* **204**, 155. (2,3).
 KUSNEZOV, D., BULGAC, A. & BAUER, W. 1992 *Annals of Physics* **214**, 180. (2,3).
 POSCH, H. A. & HOOVER, W. G. 1992 In *Molecular Liquids: New Perspectives in Physics & Chemistry* (ed. Teixeira-Dias). NATO Advanced Science Institute, vol. 20. Kluwer Academic Publishers.